Available online at www.sciencedirect.com
ScienceDirect
Catalysis Today 131 (2008) 526–532
CATALYSIS TODAY
www.elsevier.com/locate/cattod

Accurate low-pressure kinetics for isobutane oxidation over phosphomolybdic acid and copper(II) phosphomolybdates

Shane M. Kendell [a], Trevor C. Brown [a,*], Robert C. Burns [b]

[a] *Chemistry, School of Biological, Biomedical and Molecular Sciences, University of New England, Armidale, NSW 2351, Australia*
[b] *Chemistry, School of Environmental and Life Sciences, The University of Newcastle, Callaghan, NSW 2308, Australia*

Available online 26 November 2007

Abstract

A low-pressure steady-state technique has been used to investigate the rates and mechanisms of the oxidation of isobutane over $H_3[PMo_{12}O_{40}]$, $CuH_4[PMo_{12}O_{40}]_2$, $Cu_2H_2[PMo_{12}O_{40}]_2$, $Cu_{2.5}H[PMo_{12}O_{40}]_2$, and $Cu_3[PMo_{12}O_{40}]_2$. Observed oxidation products over all catalysts are methacrolein, 3-methyl-2-oxetanone, acetic acid, carbon dioxide and water. The most selective catalyst for methacrolein formation at low temperatures (<496 °C) is $Cu_{2.5}H[PMo_{12}O_{40}]_2$, where both Cu(II) reduction and acid sites play a role. The least active catalyst at low temperatures is phosphomolybdic acid followed by $Cu_3[PMo_{12}O_{40}]_2$. This activity is reversed at higher temperatures. The 3-methyl-2-oxetanone is a unique product and is likely to be the precursor to methacrylic acid. Acetic acid is also probably a precursor to complete oxidation. Catalyst deactivation or restructuring is significant only over $H_3[PMo_{12}O_{40}]$.

Keywords: Kinetics; Cracking; Oxidation; Molecular flow; Isobutane; Methacrolein; Phosphomolybdic acid; 3-Methyl-2-oxetanone

1. Introduction

Methyl methacrylate is used extensively as a monomer in the polymer industry, but is predominantly produced via environmentally hazardous synthetic processes using the acetone cyanohydrin route [1]. Alternative pathways to methyl methacrylate include catalytic oxidation reactions via methacrolein and methacrylic acid [2]. Starting with isobutane possible overall catalytic reaction steps include three or four lattice oxygens:

$$(CH_3)_3CH + 3[O] \rightarrow CH_2{=}C(CH_3)CHO + 2H_2O$$

$$(CH_3)_3CH + 4[O] \rightarrow CH_2{=}C(CH_3)COOH + 2H_2O$$

Hence, for methacrolein formation four hydrogen atoms are abstracted from the adsorbed isobutane and one lattice oxygen atom is incorporated into the adsorbed complex. The hydrogen may diffuse through the catalyst bulk where high-valent metal cations are reduced. Acidic properties of the catalyst may also affect the yield and selectivity [2].

Phosphomolybdic acid ($H_3[PMo_{12}O_{40}]$) combined with a range of cations have been shown to be active in the heterogeneous catalytic production of methacrolein and methacrylic acid from isobutane [1,3]. These catalysts have a Keggin-type structure with a large number of lattice oxygen atoms available for insertion into hydrocarbon reactants. Four types of lattice oxygen are found in the primary structure of phosphomolybdic acid: (a) internal oxygen atoms (P–O_a) (b) bridging atoms between Mo_3O_{13} units (Mo–O_b–Mo) (c) bridging atoms within Mo_3O_{13} units (Mo–O_c–Mo) and (d) external terminal oxygen atoms (Mo=O_d). The latter three oxygen atoms are the most accessible, but extended-Hückel calculations have shown that of these, O_b is slightly more active [4]. Furthermore, the rate for the oxidative dehydrogenation of isobutyraldehyde over catalysts containing $[PMo_{12}O_{40}]^{3-}$ has been shown [4] to be dependent on the rate of metal reduction and diffusion of redox carriers into the catalyst bulk. This type of catalysis, where reaction occurs at the surface, but the inner bulk plays a role, is termed bulk type II [2]. Another consideration is the effect of lattice protons on catalytic activity [4]. The acidity is not likely to be sufficiently strong for direct protonation of the alkane, but the protons could be involved in surface alkoxy formation [5].

* Corresponding author. Tel.: +61 2 6773 2872; fax: +61 2 6773 3268.
E-mail address: Trevor.Brown@une.edu.au (T.C. Brown).

0920-5861/$ – see front matter.
doi:10.1016/j.cattod.2007.10.027

In this paper, kinetic results for the reactions of isobutane over phosphomolybdic acid and over four Cu(II) substrates ion-exchanged with $H_3[PMo_{12}O_{40}]$ are reported. A low-pressure steady-state reactor directly connected to a quadrupole mass spectrometer was used for the analyses. This technique has been recently developed and shown to accurately determine the kinetic parameters associated with zeolite protolytic cracking and dehydrogenation of isobutane [6]. The low-pressure steady-state technique provides accurate catalytic kinetic information because both secondary reactions and heat fluctuations are minimized. Accessibility of active sites, diffusion limitations and catalyst deactivation due to coke formation continue to complicate the kinetics, but the impacts of these effects are less at low pressures.

2. Experimental

The low-pressure steady-state apparatus has been described in detail [6–8]. Equal proportions of reactant gas (isobutane) and argon are pre-mixed and continuously flow through a variable leak valve, into a Pyrex Knudsen cell reactor containing the catalyst. Under these molecular flow conditions, the average number of collisions of each molecule with the catalyst is determined from the ratio of the geometric or exposed surface area of the catalyst and the exit aperture area [9]. After experiencing these gas/surface collisions, reactant and product molecules escape via the exit aperture and into a quadrupole mass spectrometer.

Five Knudsen cell reactors were used in this study with similar dimensions. Reactor volumes ranged from 8000 to 10,000 mm^3, internal surface areas from 2000 to 3000 mm^2 and exit aperture areas from 0.8 to 1.6 mm^2. Gas flow rate is measured before each experiment by recording the pressure decrease from the pressure gauge situated, in a known volume, next to the variable leak valve. The maximum reactant flow-rate into the reactor is when the pressure is sufficiently low to minimize gas/gas collisions. This occurs when the reactant mean-free-path is significantly greater than the largest dimension of the Knudsen cell [10]. Using the Lennard-Jones diameter of isobutane (0.5278 nm) [11] for the collision cross section, 32 mm for the mean-free-path (typical length of reactor) and 0.8 mm^2 for the exit aperture area, one finds that the maximum isobutane flow rate at 500 °C is 4.2×10^{15} molecules s^{-1}. During an experiment the pressure within the Knudsen cell is in the range 7–10 Pa.

Instrument grade isobutane and possible gas-phase products were obtained from BOC Gases and were used without further purification. Flow rates and mass-spectral sensitivities of other products were measured using the vapor of liquid samples obtained from Sigma–Aldrich.

Hydrated phosphomolybdic acid ($H_3[PMo_{12}O_{40}]\cdot 28H_2O$) and all other reagents used in the preparation of the copper salts were obtained from Sigma–Aldrich. The salts were prepared by dissolving 12.747 g of $H_3[PMo_{12}O_{40}]\cdot 28H_2O$ in 20.0 mL of water and adding either 0.684, 1.368, 1.707 or 2.052 g of $CuSO_4\cdot 5H_2O$. Equal molar quantities of dried $BaCO_3$ were then added to the dissolved solution to precipitate the sulfate. The resultant slurry was stirred at 55 °C for 2 h and upon cooling the $BaSO_4$ was removed by filtration. Four copper-containing catalysts were the obtained by evaporating the water at 55 °C to yield green solids—$CuH_4[PMo_{12}O_{40}]_2$, $Cu_2H_2[PMo_{12}O_{40}]_2$, $Cu_{2.5}H[PMo_{12}O_{40}]_2$, $Cu_3[PMo_{12}O_{40}]_2$. The low-symmetry crystalline structures and compositions of these salts were confirmed by X-ray diffraction and fluorescence.

The typical procedure for all kinetic runs is to initially expose an accurately weighed amount (ca. 1.5 g) of one of the phosphomolybdate catalysts located within the Knudsen cell to a flow of isobutane/argon mixture for 2 h at 100 °C. At this temperature, where no reaction is apparent, the steady-state flow-rate and constant mass spectral abundances are recorded. The temperature controller is then programmed to increase the reactor temperature at 5 °C/min. Reactor temperatures and mass spectral abundances characteristic of the reactant and products are then recorded at 20 s intervals until the temperature reaches 400–450 °C. All abundances are divided by the $m/e = 20$ abundance, which is uniquely characteristic of argon.

3. Theory

The theory of heterogeneous catalysis in a Knudsen cell reactor has been previously described in detail [6]. The measurable kinetics can be divided into three elementary steps:

(i) Adsorption of gas-phase reactant R on the exposed surface of the catalyst S_{exp}

$$R_{(g)} + S_{exp} \underset{k_{-1}}{\overset{k_1}{\rightleftarrows}} S_{exp}(R) \quad \text{(R1)}$$

For some catalyst/reactant systems, dissociative adsorption occurs.

(ii) The rate-determining step for formation of gas-phase product. This could be reactant diffusion to active sites, intrinsic reaction, catalyst restructuring or product diffusion and desorption.

$$S_{exp}(R) \xrightarrow{k_2} P_{(g)} \quad \text{(R2)}$$

(iii) Escape of the product from the Knudsen cell through the exit aperture with rate constant k_{eP}.

$$P_{(g)} \xrightarrow{k_{eP}} \text{Mass spectrometer} \quad \text{(R3)}$$

The rate of appearance of product in the mass spectrometer will be [6,9]

$$\frac{d[P_{(g)}]}{dT} = \frac{I_P}{\beta \alpha_P} = \frac{k_{eP}}{\beta}[P_{(g)}] = k_2 N(R)^n \quad (1)$$

Here I_P is the abundance of a characteristic mass-spectral product, α_P is the measured sensitivity factor for converting product abundance to flow rate, β is the linear heating rate, $N(R)$ is the number of reactant species at active sites and n is the reaction order.

The main challenge with using Eq. (1) to interpret the low-pressure steady-state experiments is the accurate determination

of $N(\mathrm{R})$. This is because the number of reactant species at active sites decreases as the temperature increases. Equilibrium adsorption predicates such a decrease, but catalyst deactivation and diffusion limitations exacerbate this decrease. As a first approximation $N(\mathrm{R})$ is estimated from the Langmuir adsorption isotherm, θ_R

$$N(\mathrm{R}) = \theta_\mathrm{R} N(\mathrm{act}) = \frac{k_1/k_{-1}[\mathrm{R}_{(g)}]}{1 + k_1/k_{-1}[\mathrm{R}_{(g)}] + k_2/k_{-2}[\mathrm{P}_{(g)}]} N(\mathrm{act}) \tag{2}$$

where $N(\mathrm{act})$ is the total number of active sites. Summation is required in the denominator to include adsorption and desorption of all products. The ratio of rate constants for adsorption and desorption consist of an enthalpy of adsorption and a ratio of pre-exponential factors. For reactant adsorption the pre-exponential factor (A_1) is the collision frequency per molecule per catalyst site [6,9]

$$A_1 = \frac{A_\mathrm{S}}{A_\mathrm{h} N(\mathrm{act})} k_\mathrm{eR} \tag{3}$$

where A_S is the geometric surface area of the catalyst. Geometric surface areas were measured for each catalyst/reactor system and were in the range 130–370 mm^2. As steady-state concentrations of gas-phase species are proportional to mass-spectral abundances as shown in Eq. (1), the coverage now becomes

$$\theta_\mathrm{R} = \frac{(A_\mathrm{S}/A_\mathrm{h}A_{-1})(I_\mathrm{R}/\alpha_\mathrm{R}N(\mathrm{act}))\exp(-\Delta H_1/RT)}{1 + (A_\mathrm{S}/A_\mathrm{h}A_{-1})(I_\mathrm{R}/\alpha_\mathrm{R}N(\mathrm{act}))\exp(-\Delta H_1/RT) + (A_\mathrm{S}/A_\mathrm{h}A_{-2})(I_\mathrm{P}/\alpha_\mathrm{P}N(\mathrm{act}))\exp(-\Delta H_2/RT)} \tag{4}$$

The magnitudes of A_S, A_h, I_R, α_R, I_P, α_P and T can all be accurately measured. Reactant sensitivity factors are calculated daily, but the factors for products are less frequently measured and so are less accurate. Generic values are used for A_{-1} and A_{-5} ($10^{12\pm1}$ s^{-1} [12]). Adsorption enthalpies on these catalysts are not known and so magnitudes reported for adsorption on zeolites were initially used [13]. These values are not sensitive to the kinetic data and a simplified first approximation to the coverage is:

$$\theta_\mathrm{R} = \frac{I_\mathrm{R}/\alpha_\mathrm{R}}{1 + (I_\mathrm{R}/\alpha_\mathrm{R}) + (I_\mathrm{P}/\alpha_\mathrm{P})} \tag{5}$$

Under low-pressure conditions the coverage is low and all sites are not equally active. However, the dominant term in Eq. (5), at low temperatures, is $I_\mathrm{R}/\alpha_\mathrm{R}$, which appears in both the numerator and denominator. Thus, prior to reaction, the coverage is in effect also set equal to unity. As reactant abundance decreases and product formation increases, the reactant coverage also decreases.

The general shape of the temperature-dependent coverage is shown in Fig. 1, but the approximations used to calculate coverage mean that the magnitude of the decrease is likely to be inaccurate. Also, during temperature-programming reactant diffusion rates and blocking of active sites are likely to affect the coverage. Repeat experiments on the same catalyst indicate that deactivation is not apparent. In order to account for non-steady-state effects as well as inaccuracies in selected enthalpies of adsorption and in pre-exponential factors, an exponent m is introduced into Eq. (5), i.e. $(\theta_\mathrm{R})^m$ [6]. By combining Eqs. (1) and (2) and including m:

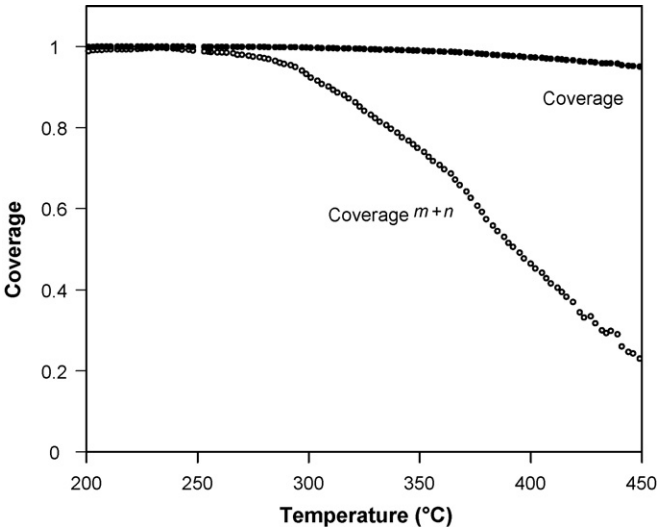

Fig. 1. Initial and optimized isobutane coverages on active sites, for methacrolein formation over phosphomolybdic acid. The optimized coverage includes the exponent $m + n = 28.9$.

$$I_\mathrm{P} = \beta\alpha_\mathrm{P}A_2(\theta_\mathrm{R})^{m+n}N(\mathrm{act})^n \exp\left(\frac{-E_2}{RT}\right) \tag{6}$$

Unknowns are E_2, A_2 and m. However, a consequence of including m and of assuming that the coverage is unity and constant at low conversions is that the apparent enthalpy of adsorption is effectively set to zero [14]. Hence, the activation energy E_3 is the apparent activation energy:

$$E_\mathrm{app} = E_3 + \Delta H_1 \tag{7}$$

Similarly, the intrinsic pre-exponential factor is replaced by the apparent pre-exponential factor is the intrinsic A_3 multiplied by the coverage prefactor in the numerator in Eq. (4):

$$A_\mathrm{app} = A_3 \times \frac{A_\mathrm{S}}{A_\mathrm{h}A_{-1}} \frac{I_\mathrm{R}^\circ}{\alpha_\mathrm{R}N(\mathrm{act})} \tag{8}$$

Here, I_R° is the mass-spectral abundance of the characteristic reactant peak when no reaction is occurring. By including E_app and A_app and taking the natural logarithm, Eq. (6) becomes

$$\ln I_\mathrm{P} = -\frac{E_\mathrm{app}}{RT} + (m+n)\ln\theta_\mathrm{R} + \ln(\beta\alpha_\mathrm{P}A_\mathrm{app}N(\mathrm{act})^n) \tag{9}$$

The solutions to a multiple linear regression analysis, using the module in MS Excel, with $\ln I_\mathrm{P}$ as the input Y data, $1/RT$ and $\ln(\theta_\mathrm{R})$ the input X data are the variables $-E_\mathrm{app}$, $m + n$ and intercept $\ln(\beta\alpha_\mathrm{P}A_\mathrm{app}N(\mathrm{act})^n)$. If $m + n$ is known, then a plot of $\ln(I_\mathrm{P}/(\theta_\mathrm{R})^{m+n})$ against $1/RT$ should be linear with intercept $\ln(\beta\alpha_\mathrm{P}A_\mathrm{app}N(\mathrm{act})^n)$ and slope $-E_\mathrm{app}$.

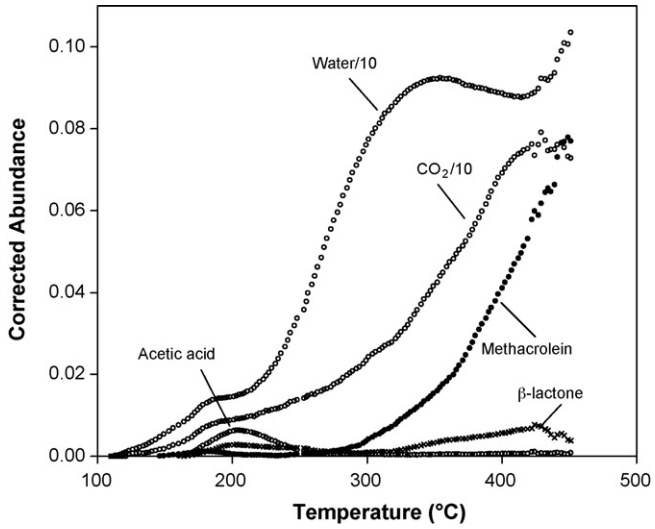

Fig. 2. Corrected mass-spectral abundances for water, carbon dioxide, acetic acid methacrolein and 3-methyl-2-oxetanone (β-lactone) formation during temperature-programmed reaction over phosphomolybdic acid.

4. Results

At least four temperature-programmed experiments were performed for each catalyst and isobutane combination. The mass-spectral data from first runs on each catalyst were not used in the calculations, because adsorbed water and other calcination effects gave results that were not consistent with later runs. Subsequent experiments on each catalyst were indistinguishable and provided the error ranges for calculated Arrhenius parameters. Over all phosphomolybdate catalysts the major gas-phase products detected by careful analysis of the mass-spectral scans are methacrolein, carbon dioxide and water. Characteristic mass-spectral peaks for these products are $m/e = 70$, 44 and 18 respectively, and temperature-dependent abundances are plotted in Fig. 2 for isobutane catalysis over phosphomolybdic acid. Water production proceeds through two points of inflection, with plateaus at 180 and 350 °C. Methacrolein rises approximately exponentially with temperature, and it is this shape that allows kinetic analyses.

Fig. 2 also shows that the formation of acetic acid ($m/e = 60$) over the temperature range 150–300 °C reaches a maximum at ca. 200 °C. The increasing rate of CO_2 formation occurs simultaneously with decreasing acetic acid evolution. A fifth gas-phase product, apparent at temperatures greater than 300 °C over phosphomolybdic acid is assigned to a β-lactone, 3-methyl-2-oxetanone. This product is identified by the characteristic mass-spectral peak, $m/e = 68$. Other evidence supporting the formation of this β-lactone is provided in Section 5. The addition of copper to the catalysts quenches the production of both acetic acid and the β-lactone and significantly reduces the formation of complete oxidation products, water and CO_2.

Propene, isobutene, 2-methyl-1-propanol and methacrylic acid could not be detected in any mass-spectral scans. Isobutane abundances ($m/e = 58$) remain approximately constant over the temperature range for all catalysts, which indicates low isobutane conversion levels under the conditions of the experiments.

Initial calculations for the coverage of isobutane complexes at active sites (Eq. (5)) used estimated mass spectral calibration and sensitivity factors from a previous study [6]. These coverages are shown in Fig. 1 for the data plotted in Fig. 2. Also shown in Fig. 1 are the coverages adjusted by the exponent $m + n$, which have been determined by a multiple linear regression analysis of Eq. (9) for methacrolein formation.

Other parameters obtained from the regression analysis for methacrolein formation over all catalysts are $-E_{app}$ and $\ln(\beta\alpha_P A_{app} N(\text{act})^n)$ and these are listed in Table 1. Errors in all parameters are calculated from the regression analysis and from a comparison of magnitudes from at least three temperature-programmed experiments.

The standard, uncorrected Arrhenius plots ($\ln k = \ln(I_P/\theta_R)$ against $1/RT$) for methacrolein formation from isobutane over phosphomolybdic acid are shown as unfilled circles in Fig. 3. Also plotted (filled circles) are $\ln(I_P/(\theta_R)^{m+n})$ against $1/RT$ for both pathways. This demonstrates the effect of linearizing the data at higher temperatures by including the optimized $m + n$ parameter. Lines are the resultant Arrhenius equations ($\ln k = E_{app}/RT + \ln(\beta\alpha_P A_{app} N(\text{act}))^n$ against $1/RT$).

5. Discussion

5.1. Product selectivity

Because molecular oxygen is absent from the reactant gas stream, the phosphomolybdate substrates act as reactants by providing lattice oxygen to facilitate product formation. Commercial applications and other studies [15] have used gas-phase oxygen to replenish lattice framework oxygen, and product selectivity can be dependent on the reactant/molecular oxygen ratio.

The selectivity of the desired product, methacrolein from isobutane is enhanced by the addition of copper(II) ions to the

Table 1
Rate parameters obtained from the multiple linear regression analysis of Eq. (9) for methacrolein formation from isobutane

Catalyst	T range (°C)	$\log_{10}(\beta\alpha_P A_{app} N(\text{act})^n)$	E_{app} (kJ mol^{-1})	$m + n$
$H_3[PMo_{12}O_{40}]$	246–451	6.21 ± 0.10	99.3 ± 1.1	28.9 ± 1.3
$CuH_4[PMo_{12}O_{40}]_2$	353–502	3.62 ± 0.08	61.3 ± 1.8	1.1 ± 0.6
$Cu_2H_2[PMo_{12}O_{40}]_2$	325–501	3.44 ± 0.13	58.4 ± 0.9	1.1 ± 0.7
$Cu_{2.5}H[PMo_{12}O_{40}]_2$	329–501	3.0 ± 0.2	52 ± 4	1.9 ± 1.4
$Cu_3[PMo_{12}O_{40}]_2$	342–500	4.59 ± 0.10	75.4 ± 1.2	1.0 ± 0.4

Units for the pre-exponential factor are $\log_{10}$(mass spectral abundance).

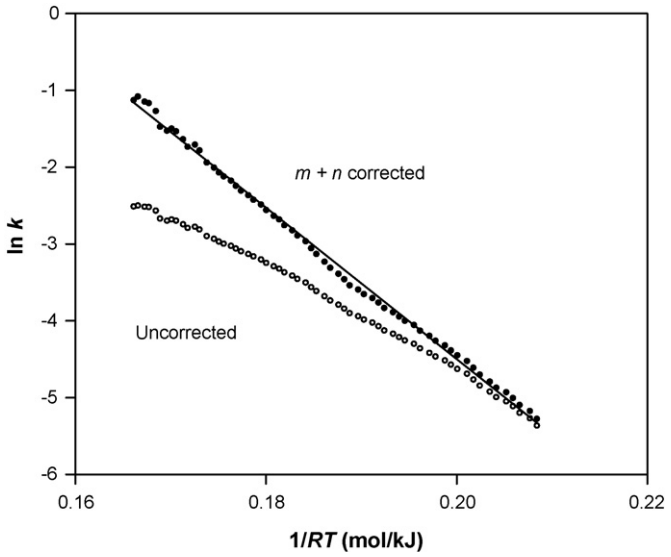

Fig. 3. Arrhenius plots of ln k against $1/RT$ for methacrolein formation over phosphomolybdic acid. Unfilled circles are the raw experimental rate constants and filled circles are the experimental data with coverage corrected by the exponent $m + n$.

phosphomolybdic acid catalysts. Also the propensity for complete combustion of isobutane is decreased, and the formation of unwanted acetic acid is quenched. Oxidation of alkanes, using molybdates, leads to one or two electron reduction of molybdenum from +6 to +5 or +4 [16]. Added copper may also reduce from +2 to +1 and facilitate the rapid transfer of electrons between anions and the bulk [4,17]. This can explain the enhanced selectivity to methacrolein, and is reflected in the observed trend of increased methacrolein formation with increased copper(II) substitution. However, the fully substituted copper(II) substrate is the least active at low temperatures, which indicates that Bronsted acidity plays a role in product selectivity [17]. The lower temperatures required for methacrolein formation [18] leads to lower isobutane coverages and hence reduced yields of acetic acid and CO_2.

Methacrolein, acetic acid and the β-lactone appear to form in parallel independent reaction mechanisms, with no apparent decrease in one of these products and increase in another as the temperature increases. Acetic acid and CO_2, however, evolve in consecutive reactions. Hence, acetic acid is likely to be an intermediate for CO_2 formation [19].

$$(CH_3)_3CH \xrightarrow{5[O]\text{-}H_2O} 2CH_3COOH \xrightarrow{8[O]} 4CO_2 + 4H_2O$$

Methacrylic acid is an expected product for the catalytic conversion of isobutane over phosphomolybdic acid, however, it is not detected under the molecular flow conditions employed in this work. The appearance of a mass-spectral peak at $m/e = 68$ was not expected. An extensive search of mass-spectral databases showed that 4-methyl-2-oxetanone was the closest match to the mass-spectral profile, however its formation from isobutane is not feasible. The formation of the isomer, 3-methyl-2-oxetane, with the methyl group diagonal across the four-member ring from the C=O, is plausible. This mass spectrum is not available, but should be analogous to the 4-methyl-2-oxetanone. Four lattice oxygen atoms are required to form this β-lactone.

$$(CH_3)_3CH \xrightarrow{4[O]} CH_3CHCH_2OC(O) + 2H_2O$$

The stability of three possible products, 3-methyl-2-oxetanone, methyl cyclopropene (parent $m/e = 68$) and methacrylic acid have been computationally analyzed using Spartan' 04. Geometries were optimized using the Hartree-Fock molecular orbital method with 6-31G* all-electron basis sets and then more rigorously using B3LYP density functional methods with the same basis sets. In order to compare the ground state energies of methylcyclopropenone with 3-methyl-2-oxetanone and methacrylic acid, the water molecule must be included in the calculations. Energies relative to methacrylic acid are listed in Table 2.

Density functional energy calculations indicate that methylcyclopropenone formation is unlikely as it exists at a much higher energy than methacrylic acid. The β-lactone, however, has a comparable energy to, but 25.42 kJ mol^{-1} higher than methacrylic acid. A simple ring opening of the β-lactone and hydrogen shift from carbon to one of the oxygen atoms can lead to the acid. Methacrylic acid is not observed under the low-pressure conditions. Other higher-pressure studies have shown that methacrylic acid is a product [1,2,4,15,17] and so β-lactone formation may be obscured by rapid acid-catalyzed conversion to methacrylic acid. Formation of the β-lactone from the heterogeneous catalysis of isobutane has not previously been reported.

5.2. Rate parameters for the formation of methacrolein

The apparent activation energy for isobutane conversion into methacrolein over phosphomolybdic acid is 99.3 ± 1.1 kJ mol^{-1}. This is similar in magnitude to the Mo^{6+} reduction energy of 90.4 kJ mol^{-1} determined by Paul et al. [20] over $(Cs^+/NH_4^+/H^+)_4[PMo_{11}VO_{40}]$. Hence the rate-determining step may be Mo^{6+} reduction. Lowering of the apparent activation energy with the addition of copper(II), would be the combined affect of Cu^{2+} and Mo^{6+} reduction. The relationship between activation energy decrease and copper(II) content is not linear, but under the low-pressure conditions not all of the Cu^{2+} is equally accessible.

Fig. 4 is a plot of the temperature-programmed rate constant profiles for methacrolein formation over each of the catalysts. Simulated rate constants calculated from the parameters listed in Table 1, without the $m + n$ correction, are used in the plots.

Table 2
Relative energies of possible products from the oxidation of isobutane over phosphomolybdates

Possible products	Relative energy (kJ/mol)
Methacrylic acid	0.00
3-Methyl-2-oxetanone	25.42
Methylcyclopropenone + water	373.50

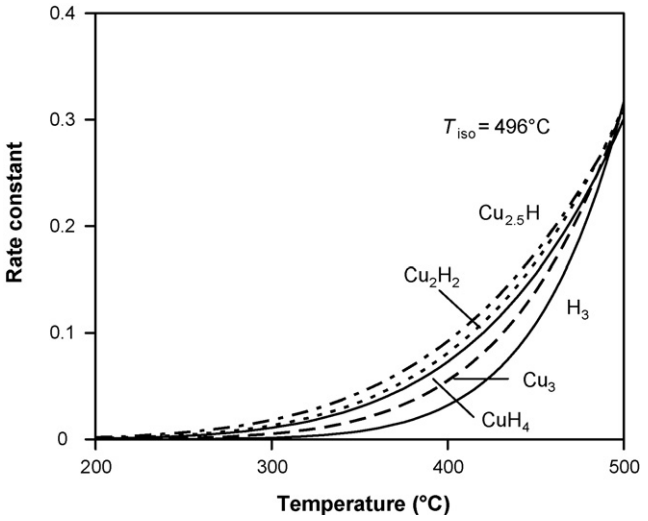

Fig. 4. Modelled rate constants for methacrolein formation over $H_3[PMo_{12}O_{40}]$, $CuH_4[PMo_{12}O_{40}]_2$, $Cu_2H_2[PMo_{12}O_{40}]_2$, $Cu_{2.5}H[PMo_{12}O_{40}]_2$, and $Cu_3[PMo_{12}O_{40}]_2$.

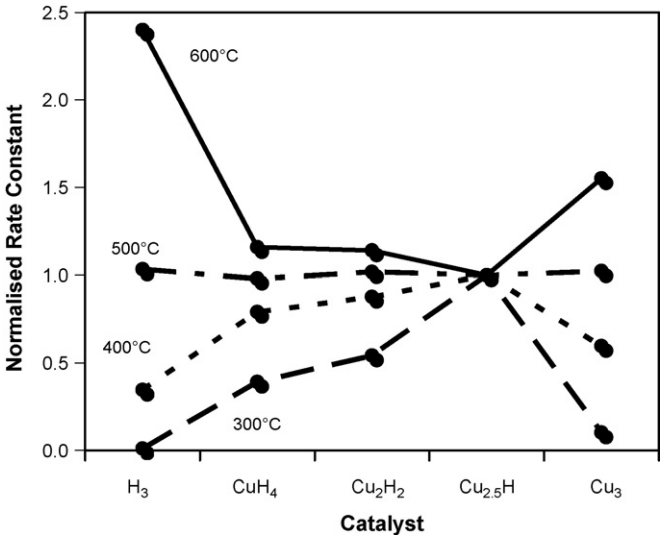

Fig. 6. Plot of methacrolein formation rate constants at 300, 400, 500 and 600 °C against the five catalysts: $H_3[PMo_{12}O_{40}]$, $CuH_4[PMo_{12}O_{40}]_2$, $Cu_2H_2[PMo_{12}O_{40}]_2$, $Cu_{2.5}H[PMo_{12}O_{40}]_2$, and $Cu_3[PMo_{12}O_{40}]_2$.

The $Cu_{2.5}H[PMo_{12}O_{40}]_2$ substrate is clearly the most active to temperatures up to ca. 496 °C. This is followed by $Cu_2H_2[PMo_{12}O_{40}]_2$, $CuH_4[PMo_{12}O_{40}]_2$, $Cu_3[PMo_{12}O_{40}]_2$ and $H_3[PMo_{12}O_{40}]$, which is the least active.

Catalyst activity is more clearly demonstrated by the Arrhenius plots in Fig. 5. These straight lines intersect at the isokinetic temperature, 496 ± 10 °C. This temperature can be related to a frequency of the transition state or resonance frequency of the solid catalyst, which has been derived using stochastic models [21], transition-state theory [22], and a dynamic model [23]. The frequency ($c\omega$) is given by

$$\omega = \frac{RT_{iso}}{Nhc} \tag{10}$$

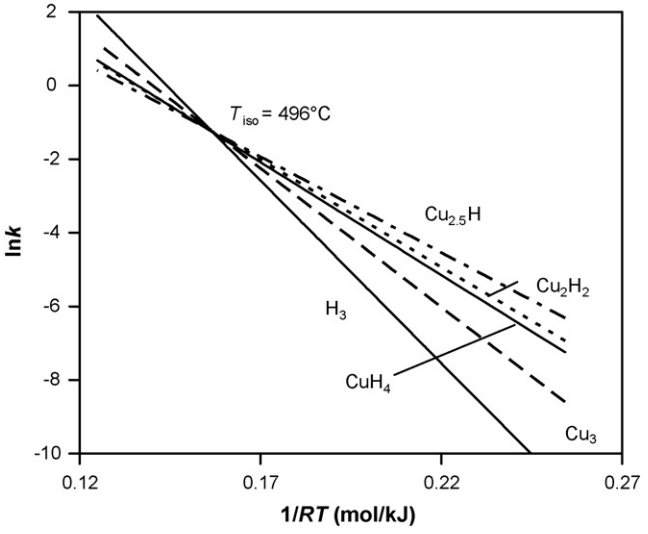

Fig. 5. Isokinetic relationship for methacrolein formation over $H_3[PMo_{12}O_{40}]$, $CuH_4[PMo_{12}O_{40}]_2$, $Cu_2H_2[PMo_{12}O_{40}]_2$, $Cu_{2.5}H[PMo_{12}O_{40}]_2$, and $Cu_3[PMo_{12}O_{40}]_2$.

For the isokinetic relationship plotted in Fig. 5 the characteristic frequency occurs at 535 ± 7 cm^{-1}. Methacrolein has several bending and wagging bands in its infrared absorption spectrum that are in the vicinity of this frequency. This suggests that these vibrations play a role in methacrolein formation from the oxidation of isobutane.

Another representation of the simulated rate constants is shown in Fig. 6. Here the rate constants relative to the $Cu_{2.5}H[PMo_{12}O_{40}]_2$ value at five temperatures are plotted against the five catalysts. From this figure it is apparent that $Cu_{2.5}H[PMo_{12}O_{40}]_2$ is the most active at 300 and 400 °C, but the least active at 600 °C.

Calculated values for $m + n$, for all copper(II) catalysts, are sufficiently close to unity to indicate that the reaction order with respect to coverage is one and catalyst deactivation or other transient effects are minimized during temperature programming. However, for the methacrolein formation over $H_3[PMo_{12}O_{40}]$, $m + n$ is significantly greater than one, i.e. 28.9 ± 1.3. The implication is that either catalyst deactivation is rapid or active sites quickly become inaccessible on the pure acid catalyst. Repeated temperature-programmed runs on the same catalyst do not show any deactivation, and so the catalyst is regenerated during cooling, perhaps by restructuring. Hence in addition to increasing methacrolein selectivity the added copper(II) decreases deactivation rates at least at low isobutane pressures.

6. Conclusions

A recently developed low-pressure steady-state technique [6] has been used to monitor the kinetics of the oxidation of isobutane over $H_3[PMo_{12}O_{40}]$, $CuH_4[PMo_{12}O_{40}]_2$, $Cu_2H_2[PMo_{12}O_{40}]_2$, $Cu_{2.5}H[PMo_{12}O_{40}]_2$, and $Cu_3[PMo_{12}O_{40}]_2$. The Cu(II)/Mo(VI) molar ratio increases from 0 to 0.125 across this series. In all cases, the measured products are methacrolein, 3-methyl-2-oxetane, acetic acid, carbon dioxide and water. The

temperature-programmed mass-spectral data for methacrolein formation are sufficiently exponential to allow accurate calculations of rate parameters.

The rate of selective oxidation to methacrolein is enhanced by the addition of copper(II) ions, while the rate of acetic acid, carbon dioxide and water formation is reduced. This is likely to be related to the reduction rate of Cu^{2+} to Cu^{1+}. The decreased methacrolein selectivity over $Cu_3[PMo_{12}O_{40}]_2$ is probably due to the absence of acid sites.

The apparent evolution of 3-methyl-2-oxetanone is a unique and plausible product from the oxidation of isobutane. Furthermore, it may be the precursor to methacrylic acid.

Calculated rate parameters for methacrolein formation show that at low temperature (<496 °C) the catalytic activity decreases from $Cu_{2.5}H[PMo_{12}O_{40}]_2 > Cu_2H_2[PMo_{12}O_{40}]_2 > CuH_4[PMo_{12}O_{40}]_2 > Cu_3[PMo_{12}O_{40}]_2 > H_3[PMo_{12}O_{40}]$, while the reverse order is the activity at temperatures greater than 496 °C.

Values of $m + n$ for methacrolein formation are close to unity for all copper(II) containing catalysts indicate that deactivation and non-steady-state processes, such as diffusion, are not affecting the rate. For $H_3[PMo_{12}O_{40}]$, $m + n = 28.9 \pm 1.3$ and so deactivation is significant or other transient effects are continuously decreasing the rate during temperature programming.

Acknowledgements

Financial support from University of New England Research Grants is gratefully acknowledged. Shane Kendell is also appreciative of a UNE postgraduate scholarship.

References

[1] F. Cavani, R. Mezzogori, A. Pigamo, F. Trifiro, Top. Catal. 23 (2003) 119–124.
[2] N. Mizuno, M. Misono, Chem. Rev. 98 (1998) 199–217.
[3] G.-P. Schindler, C. Knapp, T. Ui, K. Nagai, Top. Catal. 22 (2003) 117–121.
[4] J. Hu, R.C. Burns, J. Catal. 195 (2000) 360–375.
[5] J.F. Haw, Phys. Chem. Chem. Phys. 4 (2002) 5431–5441.
[6] C. Le Minh, T.C. Brown, Appl. Catal. A 310 (2006) 145–154.
[7] Y. Sun, T.C. Brown, J. Catal. 194 (2) (2000) 301–308.
[8] Y. Sun, T.C. Brown, Int. J. Chem. Kinet. 34 (8) (2002) 467–480.
[9] D.M. Golden, G.N. Spokes, S.W. Benson, Angew. Chem. Int. 12 (1973) 534–546.
[10] D.D. Do, Adsorption Analysis: Equilibrium and Kinetics, Series on Chemical Engineering, vol. 2, ICP, 1998.
[11] R.C. Reid, J.M. Prausnitz, B.E. Poling, The Properties of Gases and Liquids, McGraw-Hill, New York, 1987.
[12] I.G. Pitt, R.G. Gilbert, K.R. Ryan, J. Chem. Phys. 102 (8) (1995) 3461–3473.
[13] L. Dixit, T.S.R. Prasada Rao, J. Chem. Inf. Comput. Sci. 39 (2) (1999) 218–223.
[14] A.W. Adamson, Physical Chemistry of Surfaces, fifth ed., Wiley, 1990,, p. 425.
[15] F. Cavani, R. Mezzogori, A. Pigamo, F. Trifiro, E. Etienne, Catal. Today 71 (2001) 97–110.
[16] N. Ohler, A.T. Bell, J. Phys. Chem. B 109 (2005) 23419–23429.
[17] M. Langpape, J.M.M. Millet, U.S. Ozkan, P. Delichere, J. Catal. 182 (1999) 148–155.
[18] S.M. Al-Zhahrani, N.O. Elbashir, A.E. Abasaeed, M. Abdulwahed, Catal. Lett. 69 (2000) 65–70.
[19] J. Barbier, L. Oliviero, B. Renard, D. Duprez, Top. Catal. 33 (2005) 77–86.
[20] S. Paul, V. Le Courtois, D. Vanhove, Ind. Eng. Chem. Res. 36 (1997) 3391–3399.
[21] W. Linert, R.F. Jameson, Chem. Soc. Rev. 18 (1989) 477–505.
[22] J.J. Rooney, Catal. Lett. 50 (1998) 15.
[23] R. Larsson, Appl. Catal. A 167 (1998) N12–N13.